nature nanotechnology

SUPPLEMENTARY INFORMATION

DOI: 10.1038/NNANO.2017.85

In the format provided by the authors and unedited.

A solid-state single-photon filter

Lorenzo De Santis, Carlos Antón, Bogdan Reznychenko, Niccolo Somaschi, Guillaume Coppola, Jean Senellart, Carmen Gómez, Aristide Lemaître, Isabelle Sagnes, Andrew G. White, Loïc Lanco, Alexia Auffeves and Pascale Senellart

Influence of the pulse length on the reflectivity contrast and second order correlation function.

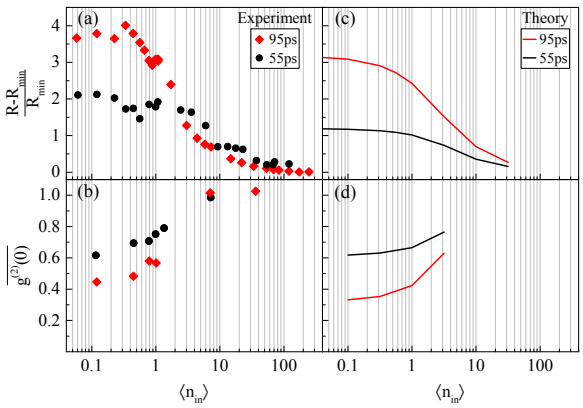

Supplementary Fig. 1: Dependence on the pulse temporal length (Device 2). (a) Measured reflectivity contrast as function of $\langle n_{\rm in} \rangle$ for 52 ps (black circles) and 94 ps (red diamonds) excitation pulses. (b) Measured second-order correlation measurements at zero delay for 52 ps (black circles) and 94 ps (red diamonds) excitation pulses. (c),(d) Corresponding calculated curves.

We present here experimental data measured on another QD-cavity device (device 2) presenting the following parameters: $\eta_{\rm top}$=63.5 ± 3%, g=19 ± 2 μeV, γ=0.5 ± 0.1 μeV and κ=100±10 μeV . The exciton fine structure splitting for this QD is $\Delta_{\rm FSS}$=10±3 μeV and the relative orientation of the QD and cavity axes θ=20°. The cooperativity is $C=g^2/(\kappa\gamma)\approx 7$. Supplementary Fig. 1(a,b) present the measured and calculated reflectivity contrast $\frac{R-R_{min}}{R_{min}}$ as a function of the average incident photon number $\langle n_{\rm in} \rangle$ for two different pulse lengths. R_{min} is the reflectivity at saturation. Supplementary Fig. 1(c,d) present the corresponding measured and calculated $\overline{g^{(2)}(0)}$.

Supplementary Fig. 1(a) shows how a longer excitation pulse – and closer to the exciton

lifetime – improves the nonlinear response of the device. Going from a 55 ps to a 95 ps pulse length, the contrast of the curve $\frac{R_{max}-R_{min}}{R_{min}}$ increases from 1.9 to 3.8 and, at the same time, the nonlinearity threshold decreases from $\langle n_{\rm in}\rangle \approx 2$ to $\langle n_{\rm in}\rangle \approx 0.5$. The narrower spectrum of the 95 ps pulse allows to limit the light directly reflected by the cavity, while exciting more efficiently the QD transition. The same effect is revealed in Supplementary Fig. 1(b), where the $\overline{g^{(2)}(0)}$ for the light reflected at low incident photon number achieves a lower value of 0.44 for the longer pulse, thanks to the presence of a higher fraction of light re-emitted by the QD.

Note that excessively long pulses have the opposite effects on the $\overline{g^{(2)}(0)}$. When the pulse length exceeds the exciton lifetime, the probability of multiple photon emission within the same pulse increases, degrading the value of the measured $\overline{g^{(2)}(0)}$.

Raw histograms on the three-photon correlation measurements

Supplementary Fig. 2 shows the raw two-dimensional histogram map of Fig. 4(a) of the main text; it corresponds to the three-photon coincidences of the incident laser (rendering a homogeneous distribution of correlation peaks) detected in SPADs 1, 2 and 3, at different relative delays, τ_{12} and τ_{23} (see description of the detection setup described in Fig. 2(b) of the main text, configuration C).

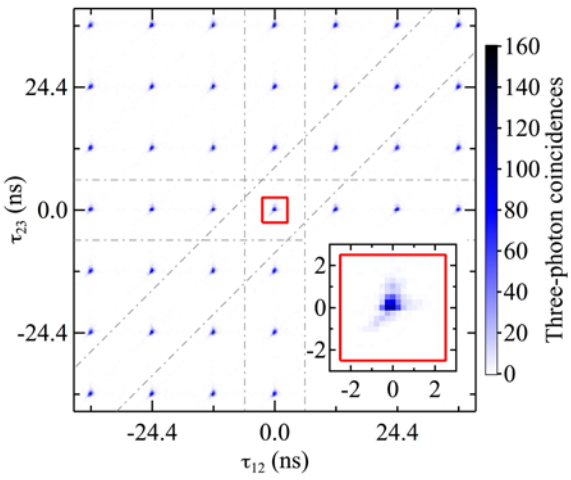

Supplementary Fig. 2: Three-photon coincidence map as function of the relative delays between detectors 1-2 (bottom axis) and 2-3 (vertical axis). The two-dimensional time bin for the coincidences detection is 256×256 ps^2.

The figure shows the region of the three-photon coincidences up to a maximum relative delay of ± 3 pulses, but the measured histograms maps are generated over relative time delays of ± 0.5 μs.

The integration area for each peak, extended over 5×5 ns^2, is marked, as an example, with a red line around the zero delay peak. It must be mentioned that the integration area is more than 5 times bigger than the temporal area of the correlation peaks. As described in the Methods section, we work in the Time-Tagged Time-Resolved mode of the correlator, and we choose a three-fold coincidences time bin of 256 ps, clearly visible in the bottom-right inset of the figure. The asymmetry of the peaks arises from the slightly different response time of each SPAD.

Theory

The QD is modeled as a three-level system involving the ground state $|G\rangle$ and two linear excitons $|X\rangle$ and $|Y\rangle$ of respective transition frequencies ω_X and ω_Y and fine-structure splitting Δ_{FSS}. The spontaneous emission and dephasing rates (taken equal for both excitons) are respectively denoted γ_{sp}, and γ^*. We have considered two quasi-resonant modes of the cavity a_H and a_V of respective polarizations H and V. Both modes have the same width κ and are equally coupled to both excitonic transitions with the parameter g. The angle between the QD's and cavity's natural axes is denoted θ. Finite spatial overlap between the cavity and the driving field is taken into account through the parameter η_{in}, while the mirrors' finite transmittances and losses are modeled through the parameter η_{top}. The H-polarized driving light of frequency ω is modeled by a classical, time-dependent Hamiltonian.

We have solved the Lindblad master equation for the density matrix ρ of the full QD-cavity system:

$$\dot{\rho} = \mathcal{L}[\rho] = -\frac{i}{\hbar}\left[\hat{H}, \rho\right] + D_{\gamma_{sp},\sigma_H}[\rho] + D_{\gamma^*,\Pi_{ex}}[\rho] + D_{\gamma_{sp},\sigma_V}[\rho] + D_{\kappa,a_H}[\rho] + D_{\kappa,a_V}[\rho] \qquad \text{(S1)}$$

$D_{\alpha,X}[\rho] = \alpha\left(X\rho X^\dagger - \frac{1}{2}(X^\dagger X\rho + \rho X^\dagger X)\right)$ is the Lindbladian super-operator describing the relaxation or the pure dephasing, involving the QD's operators $\sigma_V = |G\rangle\langle V|$ and $\sigma_H = |G\rangle\langle H|$. We have introduced the respective Hamiltonian of the problem

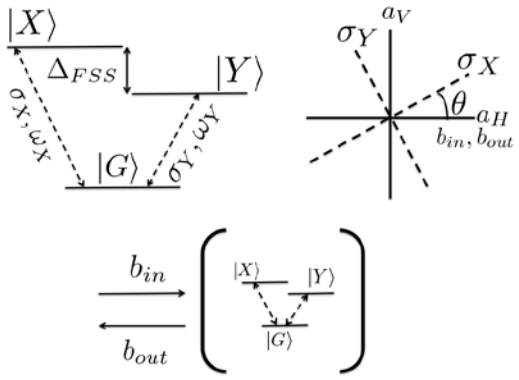

Supplementary Fig. 3: Supplementary figure 2: schematic of the model and notations. a: three level atomic system. b: relative orientations of the QD exciton axes and the cavity axes. c: input, output and cavity field operators.

$$\hat{H} = \hat{H}_{\mathrm{QD}} + \hat{H}_{\mathrm{c}} + \hat{H}_{\mathrm{i}} + \hat{H}_{\mathrm{p}} \tag{S2}$$

$$\hat{H}_{\mathrm{QD}} = \hbar(\delta_V^{\mathrm{QD}}\sigma_V^\dagger\sigma_V + \delta_H^{\mathrm{QD}}\sigma_H^\dagger\sigma_H) - \Delta_{\mathrm{FSS}}\cos(\theta)\sin(\theta)(\sigma_H^\dagger\sigma_V + \sigma_V^\dagger\sigma_H) \tag{S3}$$

$$\hat{H}_{\mathrm{c}} = \hbar(\delta_V a_V^\dagger a_V + \delta_H a_H^\dagger a_H) \tag{S4}$$

$$\hat{H}_{\mathrm{i}} = -i\hbar g(a_V\sigma_V^\dagger + a_H\sigma_H^\dagger - a_V^\dagger\sigma_V - a_H^\dagger\sigma_H) \tag{S5}$$

$$\hat{H}_{\mathrm{p}}(t) = i\hbar(\Omega^*(t)a_H - \Omega(t)a_H^\dagger) \tag{S6}$$

$\hat{H}_{\mathrm{QD}}$ is the free Hamiltonian of the QD, written as a function of the QD states

$$|V\rangle = \cos(\theta)|X\rangle + \sin(\theta)|Y\rangle \tag{S7}$$

$$|H\rangle = -\sin(\theta)|X\rangle + \cos(\theta)|V\rangle \tag{S8}$$

of respective energies $\delta_H^{\mathrm{QD}} = \delta_X\sin^2(\theta) + \delta_Y\cos^2(\theta)$ and $\delta_V^{\mathrm{QD}} = \delta_X\cos^2(\theta) + \delta_Y\sin^2(\theta)$. $\delta_X = \omega_X - \omega$ and $\delta_Y = \omega_Y - \omega$ are the respective detunings of each excitonic transition w.r. to the pump frequency, and $\Pi_{ex} = |H\rangle\langle H| + |V\rangle\langle V|$. $\hat{H}_{\mathrm{c}}$ is the free Hamiltonian of the cavity modes. $\hat{H}_{\mathrm{i}}$ is QD-cavity interaction.

The classical drive is induced by some H-polarized field injected in the input port of the

cavity mode. It acts on the QD through the Hamiltonian $\hat{H}_{\rm p}(t)$ with classical Rabi frequency

$$\Omega(t) = \sqrt{\eta_{top}\kappa}\langle \hat{b}_{in}\rangle(t) \tag{S9}$$

$$\langle b_{in}(t)\rangle = \sqrt{n_{in}}\left(\frac{4\ln(2)}{\pi\tau^2}\right)^{1/4}\exp(-2\ln(2)t^2/\tau^2) \tag{S10}$$

where $\hat{b}_{in}$ is the input field operator, $\langle a\rangle = \mathrm{Tr}\,(a\rho)$ for any operator a, and n_{in} is the mean number of photons in the pulse.

Finally, the H-polarized detected field operator $\hat{b}_{out}$ verifies the standard input-output equation:

$$\hat{b}_{out} = \hat{b}_{in} + \sqrt{\eta_{top}\kappa}\, a_H \tag{S11}$$

The theoretical value of $\overline{g^{(2)}(0)}$ was computed using the following formula:

$$\overline{g^{(2)}(0)} = \frac{\int_{-\infty}^{\infty} dt \int_{-\infty}^{\infty} d\tau G^{(2)}(t,t+\tau)}{[\int_{-\infty}^{\infty} dt \langle \hat{b}^{\dagger}_{out}(t)\hat{b}_{out}(t)\rangle]^2} \tag{S12}$$

where

$$G^{(2)}(t_1,t_2) = \langle \hat{b}^{\dagger}_{out}(t_1)\hat{b}^{\dagger}_{out}(t_2)\hat{b}_{out}(t_2)\hat{b}_{out}(t_1)\rangle \tag{S13}$$

The two-time correlations functions are derived using the Quantum Regression Theorem, such that $\langle a^{\dagger}(t)a^{\dagger}(t+\tau)a(t+\tau)a(t)\rangle = \mathrm{Tr}\left[\left(U(t,t+\tau)a\rho(t)a^{\dagger}U^{\dagger}(t,t+\tau)\right)a^{\dagger}a\right]$. We have introduced the evolution super-operator $U(t_1,t_2)$, verifying $\rho(t_2) = U(t_1,t_2)\rho(t_1)U^{\dagger}(t_1,t_2) = \int_{t_1}^{t_2} dt' \mathcal{L}[\rho(t')]$, where the expression of $\mathcal{L}[\rho(t')]$ is given in (S1).

Time evolution of the reflected intensity

Supplementary Fig. 4 shows the calculated dynamics of the intensity reflected by the device when the QD is off resonance (red trace) and on resonance (blue trace). To have a better insight of the various contributions to this signal, we consider a gaussian profile of the laser pulse of 20 ps. The average photon number per pulse is $\langle n_{\rm in}\rangle = 1$. When the QD is off resonance, the dynamics shows two peaks: the first one, A_1, corresponds to laser light which does not enter into the cavity and that is directly reflected from the top mirror because of bad spectral matching to the cavity mode. The second pulse, A_2, corresponds to light reflected after entering the cavity, its decay time corresponds to the lifetime of the cavity

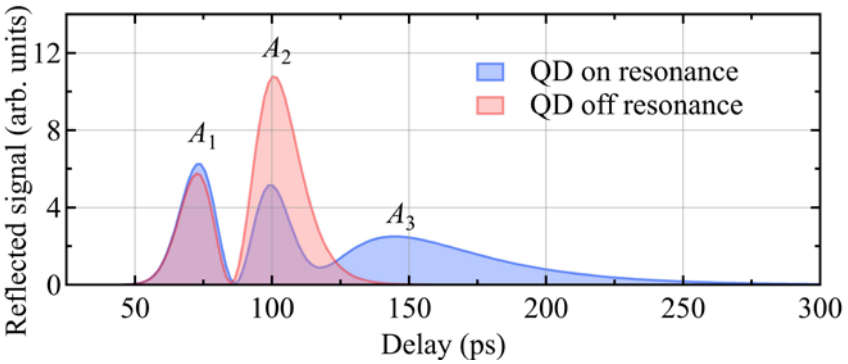

Supplementary Fig. 4: Simulation on the time evolution of the intensity reflected by device when the QD is on (blue curve) and off resonance (red curve).

photons. When the QD is on resonance with the cavity mode, a third peak A_3 appears corresponding to the re-emission of single photons by the QD. This third peak is delayed by the exciton radiative lifetime.

Effect of a power dependent electron tunneling out of the QD

In Fig. 2(a,b) of the main text, the experimental dependence of the reflected intensity and $\overline{g^{(2)}(0)}$ as function of $\langle n_{\text{in}} \rangle$ show a slightly sharper saturation curve than the simulations (solid line).

As explained in the main text, this can be attributed to a variety of phenomena. We illustrate how this behavior can for instance be reproduced considering the effect of a power dependent electron tunneling out of the QD. If the electron tunnels out of the QD, then for the next pulse, the QD will be in a charged state and the optical response will be that of an empty cavity. In practice, this would result in a progressive reduction of the probability for the QD to be in the neutral state so that the reflectivity and the $\overline{g^{(2)}(0)}$ would be given by:

$$R' = Rp_{QD} + R_c(1 - p_{QD}) \tag{S14}$$

$$\overline{g^{(2)}(0)}' = \overline{g^{(2)}(0)}p_{QD} + g_c^{(2)}(1 - p_{QD}) \tag{S15}$$

where p_{QD} is the probability for the QD to be in the neutral exciton state, and R and $\overline{g^{(2)}(0)}$ are the previously calculated values, R_c is the bare cavity reflectivity and $g_c^{(2)} = 1$ is the second order correlation function of the laser light. Using a phenomenological dependence of $p_{QD} = \frac{1}{1+\left(\frac{\langle n_{\text{in}} \rangle}{N_0}\right)^2}$ with $N_0 = 3$, allows a good description of the experimental observations (dotted lines in Figs. 2(a,b) of the main text).